THE *IRAS* BRIGHT GALAXY SAMPLE. V. MULTIBEAM PHOTOMETRY OF GALAXIES WITH $L_{IR} \geqslant 10^{11}\ L_{\odot}$

DAVID P. CARICO, D. B. SANDERS,[a] B. T. SOIFER, K. MATTHEWS, AND G. NEUGEBAUER
Palomar Observatory, California Institute of Technology, Pasadena, California 91125
Received 9 January 1990; revised 26 March 1990

ABSTRACT

Forty-seven galaxies from the *IRAS* Bright Galaxy Sample with infrared luminosities $L_{IR} \geqslant 10^{11} L_{\odot}$ have been measured at 1.3, 1.65, and 2.2 μm with beam diameters of 17″, 33″, and 55″. These measurements, combined with 5″ and 10″ observations presented in an earlier paper, provide an opportunity to study the spatial distribution of the near-infrared emission in luminous *IRAS* galaxies. It is found that the unusually red near-infrared colors known previously for many of these galaxies are confined to the nuclear regions, whereas the outer disk regions have near-infrared colors essentially appropriate for a normal stellar population. Since dust reddening and emission are required to explain the unusual nuclear colors, it follows that the observed effects of dust in these galaxies are also confined primarily to the nuclei. Thus, it is probable that the far-infrared emission, the bulk of the entire luminosity in infrared luminous galaxies, is highly concentrated about the nuclei, and that *the physical processes responsible for the unusual properties of infrared luminous galaxies tend to occur within the central regions, with diameters* $\lesssim$ *1–3 kpc.* The nuclei are found to have considerably higher 2.2 μm luminosities than are found in classical "starburst" nuclei, implying that infrared luminous galaxies are characterized by extremely high radiation densities in their central regions, presumably due to intense star-formation activity and/or the presence of a dust-enshrouded quasar. However, the nuclei of the galaxies studied are typically *not* as luminous at 2.2 μm as classical Seyfert nuclei, which may be partly attributable to extinction from dust at near-infrared wavelengths, particularly for those sources in the sample that have been identified in the literature as having Seyfert nuclei. Finally, the large diameter beam measurements are used to obtain estimates of the total near-infrared emission. It is found that, since most of the infrared luminosity is coming from the nuclei, the global near-infrared properties of infrared luminous galaxies are not good tracers of infrared activity. Also, the contribution from the observed stellar emission to the total observed luminosity is found to be $\lesssim$25% for most of the galaxies in the sample, considerably smaller than the value for typical low-luminosity spiral galaxies.

I. INTRODUCTION

The *IRAS* Bright Galaxy Sample (hereafter referred to as the BG Sample) was defined by Soifer *et al.* (1987) in order to provide a complete sample of galaxies with strong infrared emission. A revised version of the BG Sample was recently presented by Soifer *et al.* (1989) which contains 313 galaxies and is complete down to a flux limit of 5.24 Jy at 60 μm. The far-infrared emission in virtually all galaxies in the BG Sample appears to be due to thermal emission from dust grains. At the longest *IRAS* wavelengths (60 and 100 μm) the energy distributions are well modeled by steady-state dust emission. At 12 and 25 μm, however, the *IRAS* data suggest that significant quantities of very small dust grains (with radii $\lesssim$ a few tens of angstroms) which are subject to extreme temperature fluctuations from single-photon absorption events may be required to explain the observed emission (see, e.g., Boulanger *et al.* 1988; Telesco, Decher, and Joy 1989; Helou 1986).

Infrared measurements from 1 to 10 μm for most of the galaxies from the original BG Sample (Soifer *et al.* 1987) with infrared luminosities* $L_{IR} \geqslant 10^{11}\ L_{\odot}$ were presented by Carico *et al.* (1988) (hereafter referred to as Paper I), and those galaxies with $L_{IR} \geqslant 10^{12}\ L_{\odot}$ have been studied extensively by Sanders *et al.* (1988). The results of these studies indicate that the galaxies in the BG Sample possess a broad range of galaxy properties, from those seen in normal, optically selected spiral galaxies to those typical of active galactic nuclei (AGN) and quasars. This broad range of properties is seen in the near-infrared colors measured in the central 5″–10″ diam regions of the galaxies. However, the colors that are significantly different from those seen in normal spiral galaxies appear to be limited to galaxies with infrared luminosities greater than $\sim 10^{11}\ L_{\odot}$ (Paper I).

The cause of the high luminosity for those galaxies with $L_{IR} \sim 10^{11}$–$10^{12}\ L_{\odot}$ appears to be star formation (Sanders *et al.* 1986), and the broad range in near-infrared colors is presumably due to the effects of dust absorption (reddening) and emission in the source. For the highest luminosities ($L_{IR} \geqslant 10^{12}\ L_{\odot}$), Sanders *et al.* (1988) have shown that virtually all of the galaxies from the BG Sample are galaxy merger remnants (see also Carico *et al.* 1990), and have suggested that such objects contain dust-enshrouded active nuclei and represent a stage in the formation of a "classical" quasar; hence, for these sources the near-infrared colors may also be affected by a contribution from the direct emission from the accretion disk of an active nucleus (see Phinney 1989; Sanders *et al.* 1989).

This paper presents new near-infrared measurements, made with multiple large beam diameters, of a sample of galaxies from the BG Sample with $L_{IR} \geqslant 10^{11} L_{\odot}$. These data, when combined with previously published small-beam measurements, provide a basis for studying the spatial distribution of the near-infrared emission in infrared-luminous galaxies. Throughout this paper, all subsequent references to

[a] Present address: Institute for Astronomy, University of Hawaii, Honolulu, HI 96822.

*L_{IR} is an estimate of the integrated luminosity between 8 and 1000 μm; see Carico *et al.* (1988). Throughout the text, H_0 is taken as 75 km s^{-1} Mpc^{-1}; $L_{\odot}$ is the solar bolometric luminosity, 3.83×10^{26} W.

 0004-6256/90/010070-14$00.90

the BG Sample, unless stated otherwise, will refer to the revised BG Sample (Soifer *et al.* 1989).

II. THE SAMPLE AND OBSERVATIONS

The revised BG Sample contains 79 galaxies with total infrared luminosities $L_{IR} \geqslant 10^{11}\ L_{\odot}$ (Soifer *et al.* 1989). In early 1987, a program was undertaken to measure as many of these 79 galaxies as possible at near-infrared wavelengths using more than one beam diameter. The goals of the program were (1) to measure the spatial distribution of the near-infrared emission in these galaxies, and (2) to obtain estimates of the *total* near-infrared emission for comparison to the *IRAS* data, for which typical beam dimensions at 60 μm were $1'.5 \times 4'.75$ (see the *IRAS Explanatory Supplement* 1988).

Three observing runs between June 1987 and April 1988 on the 60 in. telescope at the Palomar Observatory resulted in observations of 47 of the 79 galaxies (59%) at 1.27 μm (J), 1.65 μm (H), and 2.2 μm (K), using 17″, 33″, and 55″ beam diameters. A solid-nitrogen-cooled InSb detector was used for all of the measurements, and sky subtraction was achieved by chopping to reference positions ~90″ north and south of the source.

The choice of which of the galaxies with $L_{IR} \geqslant 10^{11}\ L_{\odot}$ to observe was essentially arbitrary. Not all of the galaxies were measured with all three beam sizes at all wavelengths; in particular, it was not possible to measure many of the sources at 2.2 μm with a 55″ diameter beam due to saturation of the detector from sky background. Also, the largest useful beam diameter was occasionally limited by contamination from extraneous sources near the object of interest.

Optical images indicate that many of the measured sources have severely distorted morphologies evidenced by multiple nuclei (see, for example, Sanders *et al.* 1988). In such cases, an attempt was generally made to measure all apparent nuclei. These considerations are discussed in the Notes to Table I.

The uncertainties in the flux densities range from 6% to 28%, with a median uncertainty at each wavelength of less than 10%. No attempt has been made to correct the data for reddening caused by interstellar material in the source or in the Galaxy. For many of the galaxies there is insufficient information to enable an accurate estimation of the internal reddening, and since all of the objects in the BG Sample have Galactic latitude $|b| > 30°$, Galactic reddening in the near-infrared is negligible. Also, the data have not been corrected for source redshift, since the redshift corrections are less than the measurement uncertainties in the data.

The observational data are presented in Table I, and notes on individual sources are given immediately following the table. The column entries for Table I are as follows:

(1) Most commonly used galaxy name(s).

(2)–(7) 1950 coordinates.

(8) Approximate optical diameter of the galaxy, as estimated from the Palomar Observatory Sky Survey prints by Carico *et al.* (1988).

(9) Beam position in the source.

(10), (11) Beam diameter, in arcseconds and in kiloparsecs at the source.

(12)–(14) Flux density in milliJanskys (1 Jy $\equiv 10^{-26}$ W m^{-2} Hz^{-1}).

(15), (16) Estimates of the total stellar luminosity L_* (see Sec. III*b*) and the infrared luminosity L_{IR}.

In addition to the large-beam measurements from the Palomar 60 in. telescope, Table I also includes 5″ and 10″ measurements from the Palomar 200 in. Hale telescope. These data have all been previously presented in Paper I, but are included here for convenience.

Histograms are shown in Fig. 1 of the distribution of galaxy luminosities for the galaxies listed in Table I, and for all galaxies from the BG Sample with $L_{IR} \geqslant 10^{11}\ L_{\odot}$. The figure shows that the galaxies listed in Table I are not strongly biased toward any particular luminosity range within the luminosities of the Bright Galaxies with $L_{IR} \geqslant 10^{11}\ L_{\odot}$.

III. RESULTS AND DISCUSSION

a) Spatial Distribution of the Near-Infrared Emission

1) Wavelength dependence

To understand the spatial distribution of the near-infrared emission in infrared-luminous galaxies one would, ideally, use the data in Table I to obtain near-infrared colors in all annuli to determine how these colors change with radial distance from the center of the galaxies. Unfortunately, this is not possible in general. Since the annular colors are determined by subtracting two relatively similar large numbers, the resulting uncertainties for many of the galaxies are larger than the effects attributable to different physical processes.

In order to minimize these uncertainties, the "nuclear" colors of each galaxy were defined to be those obtained with the smallest diameter beam, and the "disk" colors were defined to be those measured in the region between the smallest diameter beam, and the largest diameter beam for which measurements were made at all three wavelengths. The results are listed in Table II and plotted in Fig. 2, where only those galaxies with *both* nuclear and disk colors with uncertainties less than 33% are presented.

In Fig. 2, typical uncertainties in $\log[f_\nu(\lambda_1)/f_\nu(\lambda_2)]$ are estimated to be ± 0.04 for the nuclei and ± 0.09 for the disks (although the fact that the total scatter in the measurements of the disk colors is only ~0.1 suggests that the uncertainties in these measurements are actually somewhat less). Because of these uncertainties, a number of the galaxies have colors that are consistent with no change between the nucleus and the surrounding disk. Fifteen of the 28 sources listed in Table II have colors in the nucleus and disk that are clearly distinct. These sources are indicated with an asterisk in Table II, and for all cases the nuclei are considerably redder than the surrounding disks. Furthermore, for all 28 sources listed in Table II, the calculated f_ν (2.2 μm)/f_ν (1.6 μm) color in the nucleus is redder than that calculated for the disk. If the uncertainties are truly statistical, this color difference suggests a tendency toward redder nuclei even among the 13 galaxies for which the nuclear and disk colors cannot be formally distinguished individually.

The above result demonstrates that, for those galaxies with the reddest near-infrared continuum emission, as reported and discussed in Paper I, the excess near-infrared emission tends to be confined to the nuclei which, from Table II, puts a limit of 1–3 kpc on the diameter of the emitting region. In contrast, the colors of the surrounding regions in those galaxies are similar to the colors of a normal stellar disk. A similar result has been found previously for a number of specific "starburst" and/or active galaxies, for example NGC 1068 (Scoville *et al.* 1988), NGC 253 (Scoville *et al.* 1985), and NGC 7469 (Cutri *et al.* 1984). Also, Devereux (1989) put a limit of ~0.5 kpc on the diameter of the region responsible for the excess infrared emission from a sample of

TABLE I. Flux densities.

NAME(S)[a]	RA −1950− (h) (m) (s)	DEC (°) (′) (″)	D_0 (″)	POS[b]	BEAM DIAM (″)	(kpc)	$f_\nu(\lambda)$(mJy)[c] 1.27 μm	1.65 μm	2.23 μm	LOG[$L/L_\odot$][d] L_*	L_{IR}
NGC 34 (Mrk 938)	0 8 33.4	−12 23 10	35		5	1.9	23.02	35.44	37.17	10.85	11.41
					17	6.5	38.20	57.19	48.55		
					33	12.7	49.44	66.31	56.78		
					55	21.1	51.30	66.29			
MCG-02-01-051† (Arp 256)	0 16 18.0	−10 39 14	35	S	5	2.4	6.17	8.76	8.48		(11.07)
					17	8.2	13.00	20.49	14.94		
					33	16.0	19.15	22.92	18.80		
				N	5	2.4	1.53	1.88	1.52		(10.94)
					17	8.2	5.73	9.50	8.13		
					33	16.0	13.25	17.05	13.87		
					55	26.7	17.79	20.39			
MCG-03-04-014	1 7 42.0	−17 7 1	25		5	3.2	11.54	16.96	16.68	10.77	11.58
					17	11.0	24.33	36.61	32.98		
					33	21.4	32.07	41.70	38.21		
					55	35.7	34.21				
MCG+02-04-025†	1 17 22.8	+14 5 53	25		17	10.3	10.52	13.25	11.54	10.61	11.63
					33	19.9	21.98	17.63	18.98		
					55	33.2	16.99	23.20	21.99		
NGC 695 (UGC 1315)	1 48 28.1	+22 20 10	35		5	3.2	10.62	14.50	13.75	11.19	11.63
					17	10.7	28.71	40.06	31.79		
					33	20.9	46.79	58.16	48.55		
					55	34.8	47.22	62.93	55.75		
NGC 958	2 28 11.8	− 3 9 32	100		5	1.9	12.77	17.44	14.94	11.36[e]	11.13
					17	6.3	45.51	61.86	49.92		
					33	12.3	89.97	127.96	102.38		
					55	20.5	134.93	195.89	160.78		
NGC 1068†	2 40 7.2	+20 13 30	540		5	0.5	193.24	300.23	769.54	10.92[e]	11.26
					10	0.9	375.07	546.32	899.98		
					17	1.5	605.49	850.06	1175.53		
					33	3.0	1153.74	1532.68	1730.74		
					55	5.0	1520.92	2096.29	2219.38		
UGC 2238	2 43 33.4	+12 53 10	35		5	2.0	7.76	14.24	16.38	10.60	11.23
					17	6.9	20.05	30.39	29.80		
					33	13.3	34.84	47.74	42.29		
					55	22.2	37.51	57.57	52.75		
IRAS 0243+213	2 43 49.2	+21 22 44	20		10	4.4	13.00	17.92	16.68		11.05
					17	7.5	13.00	25.57	20.81		
					33	14.5	21.98	28.04	25.48		
					55	24.2	22.19	33.61	23.89		
UGC 2369†	2 51 15.6	+14 46 1	40	MID	55	33.3	54.21	68.78	59.46	11.06	11.57
				N	5	3.0	8.91	12.29	10.82	10.78[e]	(11.40)
					17	10.3	23.02	27.94	24.34		
					33	20.0	35.16	45.64	36.83		
				S	5	3.0	5.08	7.47	8.06	10.65[e]	(11.08)
					17	10.3	8.13	14.66	14.13		
					33	20.0	16.68	27.71	17.79		
IRAS 0335+15†	3 35 57.1	+15 23 6	20		10	6.8	4.35	5.77	5.84		11.44
					17	11.6	3.65	6.39	6.00		
					33	22.6	6.00	11.22	9.69		
					55	37.7	9.77	10.60	10.05		
UGC 2982	4 9 43.2	+ 5 25 12	35		5	1.7	8.13	13.35	13.37	10.60	11.15
					10	3.4	17.46	27.85	28.99		
					17	5.8	23.23	41.00	37.52		
					33	11.3	46.36	69.80	63.42		
					55	18.9	58.90	84.26	72.15		
MCG-03-12-002†	4 19 6.5	−18 55 48	20	N	5	3.1	6.40	8.19	9.00	10.91[e]	(11.26)
					10	6.1	11.86	16.35	15.21		
					17	10.4	14.93	22.35	18.98		
					33	20.2	26.68	34.28	27.43		
					55	33.7	39.64	51.70			
				S	5	3.1	4.55	6.75	7.08	10.41[e]	(10.95)
					10	6.1	6.83	9.58	9.51		
					17	10.4	6.00	11.87	9.34		
NGC 1614 (Mrk 617)	4 31 35.8	− 8 40 55	50		5	1.5	34.21	48.47	49.00	10.66	11.58
					10	3.1	42.28	59.90	59.46		
					17	5.2	50.36	73.66	65.80		
					33	10.1	75.53	104.25	100.52		
					55	16.9	83.58	122.01	95.99		
NGC 2623 (Arp 243)	8 35 25.2	+25 55 48	35		5	1.8	9.33	15.05	18.12	10.49	11.55
					17	6.1	19.87	27.75	27.68		
					33	11.8	28.98	45.91	32.08		
					55	19.7	29.25	46.20	38.57		

TABLE I. (continued)

NAME(S)[a]	RA −1950− (h)	(m)	(s)	DEC (°)	(′)	(″)	D_o (″)	POS[b]	BEAM DIAM (″)	(kpc)	$f_\nu(\lambda)$(mJy)[c] 1.27 μm	1.65 μm	2.23 μm	LOG[$L/L_\odot$][d] L_*	L_{IR}
MGC+08-18-012	9	33	18.5	+48	41	53	30		5	2.5	8.83	12.45	12.42	10.61	11.31
									10	5.0	14.00	18.45	17.79		
									17	8.6	14.66	19.64	14.94		
									33	16.6	21.58	28.89	24.11		
									55	27.7	21.78	32.02			
NGC 3110	10	1	32.2	− 6	14	2	60		5	1.6	11.12	15.76	14.53	10.73	11.22
									17	5.3	31.20	46.70	39.65		
									33	10.3	63.40	85.44	69.54		
									55	17.2	79.82	104.10			
IRAS 1056+24[†]	10	56	35.5	+24	48	43	25		10	8.1	11.12	15.76	16.99		11.99
									17	13.7	12.89	17.36	17.47		
									33	26.7	14.39	20.42	19.69		
									55	44.5	16.99	23.41			
A1101+41 (V 32)	11	1	5.8	+41	7	8	35		5	3.3	5.42	7.90	8.36	10.69	11.58
									17	11.4	12.65	16.83	14.53		
									33	22.1	14.00	18.67	16.68		
									55	36.8	15.64	17.92			
UGC 6436[†] (IC 2810)	11	23	9.8	+14	56	53	15	W	5	3.3	5.57	7.97	7.84	10.59	(11.38)
									17	11.2	14.00	17.28	16.38		
									33	21.8	15.49	16.11	21.79		
									55	36.4	22.39	30.86			
								E	17	11.2	4.90	4.09	3.39	10.30	(10.84)
									33	21.8	5.57	4.43	3.89		
									55	36.4	15.64	21.35			
NGC 3690[†] (Mrk 171)	11	25	42.0	+58	50	17	80		5	1.0	22.81	32.92	38.21	10.91[e]	11.90
									17	3.5	43.86	68.50	68.90		
									33	6.7	115.37	173.01	166.81		
									55	11.2	196.84	268.81			
NGC 4418 (UGC 7545)	12	24	22.1	− 0	36	14	60		5	0.7	10.73	14.11	12.31	9.82	11.10
									17	2.2	28.45	35.49	27.68		
									33	4.4	42.67	52.29	41.14		
									55	7.3	51.77	68.78			
Mrk 231 (UGC 8058)	12	54	4.8	+57	8	38	30		5	4.1	45.51	100.33	182.91	11.54	12.52
									10	8.2	48.54	101.26	189.77		
									17	13.9	48.54	110.05	177.92		
									33	26.9	64.58	124.23	204.28		
									55	44.9	66.39	114.14			
NGC 4922[†] (UGC 8135)	12	59	1.0	+29	34	59	45	MID	55	26.1	77.64	103.15		11.03	11.31
								SW	5	2.4	16.22	19.84	15.93	10.76[e]	(11.11)
									17	8.1	35.49	44.11	32.98		
									33	15.7	57.82	68.09	51.79		
								NE	5	2.4	4.64	6.88	8.75	10.61[e]	(10.89)
									17	8.1	13.25	17.39	15.93		
									33	15.7	27.17	36.75	31.21		
IC 860	13	12	40.1	+24	52	52	35		5	1.3	8.13	10.60	9.34	10.15	11.11
									17	4.3	24.33	30.95	24.56		
									33	8.3	35.82	44.58	33.90		
									55	13.8	35.16	45.86			
UGC 8335[†] (VII ZW 506)	13	13	41.3	+62	23	17	30	SE	5	3.0	7.62	11.31	12.31	10.76	(11.53)
									17	10.3	8.83	15.71	15.93		
									33	20.0	12.65	19.01	23.24		
									55	33.3	19.87	22.36			
								NW	5	3.0	4.23	6.16	6.23	10.73	(11.37)
									17	10.3	6.89	11.37	10.33		
									33	20.0	10.43	13.13	15.78		
									55	33.3	13.62	19.30			
NGC 5256[†] (UGC 8632)	13	36	14.2	+48	31	52	25	MID	17	9.1	27.68	38.99	34.53	10.98	11.47
									33	17.7	43.46	57.54	47.23		
									55	29.4	48.99	62.15			
								SW	5	2.7	7.55	11.41	11.54	10.61[e]	(11.23)
								NE	5	2.7	7.62	9.94	8.59	10.59[e]	(11.10)
NGC 5257[†] (UGC 8641)	13	37	22.1	+ 1	5	13	115		5	2.2	4.64	6.39	5.89	10.90	11.50
									17	7.5	18.12	21.78	18.80		
									33	14.5	43.06	56.06	46.80		
									55	24.2	53.72	70.71			
Mrk 273 (UGC 8696)	13	42	51.6	+56	8	13	70		5	3.7	8.59	12.99	15.21	10.83	12.14
									17	12.5	16.07	24.63	27.43		
									33	24.3	22.19	33.84	32.08		
UGC 8739	13	47	1.7	+35	30	14	110		5	1.7	5.04	9.75	11.33	10.52	11.04
									17	5.6	16.37	30.98	30.64		
									33	10.9	35.82	55.96	50.84		
									55	18.2	43.06	63.89			
ZW 247.020 (Mrk 1490)	14	17	53.8	+49	27	54	20		5	2.5	8.44	12.40	12.08	10.46	11.32
									17	8.6	13.49	18.97	18.29		
									33	16.6	13.62	21.98	17.15		
									55	27.7	15.49	22.15			

TABLE I. (continued)

NAME(S)[a]	RA –1950– (h)	(m)	(s)	DEC (°)	(′)	(″)	D_o (″)	POS[b]	BEAM DIAM (″)	(kpc)	$f_\nu(\lambda)$(mJy)[c] 1.27 μm	1.65 μm	2.23 μm	LOG[$L/L_\odot$][d] L_*	L_{IR}
UGC 9618† (Arp 302)	14	54	47.8	+24	48	58	80	N	5	3.3	6.70	12.06	14.26	10.93[e]	(11.36)
									17	11.1	11.43	16.72	14.94		
									33	21.6	34.21	48.50	46.37		
								S	17	11.1	9.16	11.05	7.98	10.73[e]	(11.31)
									33	21.6	14.93	17.87	13.25		
I ZW 107 (Mrk 848)	15	16	19.0	+42	55	41	40		5	3.9	5.62	7.47	8.06	10.91	11.85
									17	13.2	6.28	12.49	11.54		
									33	25.7	18.80	23.71	21.00		
									55	42.8	17.79	23.20			
IRAS 1525+36†	15	25	3.1	+36	9	0	20		5	5.2	2.92	3.89	3.89	10.73	12.00
									10	10.4	3.48	4.72	4.55		
									17	17.6	3.24	3.97	4.39		
									33	34.2	6.76	7.17	8.92		
									55	35.7	9.25	9.67			
Arp 220 (UGC 9913)	15	32	46.3	+23	40	8	50		5	1.8	9.16	17.44	21.79	10.67	12.19
									10	3.5	18.80	30.58	33.90		
									17	6.0	27.93	43.33	40.39		
									33	11.6	51.77	70.08	60.01		
									55	19.4	59.99	78.97			
NGC 6090† (UGC 10267)	16	10	24.0	+52	35	6	25	MID	17	9.6	25.71	23.76	21.59	10.89	11.48
									33	18.6	30.63	32.93	28.20		
									55	31.0	31.49	35.76			
								NE	10	5.6	13.00	16.65	15.50	10.74[e]	(11.35)
								SW	10	5.6	5.13	5.77	5.18	10.62[e]	(10.89)
MCG+01-42-088	16	28	27.4	+ 4	11	24	40		5	2.3	10.92	16.05	16.08	10.62	11.34
									17	7.8	27.17	35.61	32.08		
									33	15.1	35.49	45.93	44.28		
									55	25.2	30.63	41.06			
NGC 6286† (Arp 293)	16	57	44.9	+59	0	40	65		10	3.6	17.62	28.15	30.08	10.73	11.32
									17	6.2	28.45	48.06	45.94		
									33	12.0	48.54	72.98	65.20		
									55	19.9	57.29	85.01			
IRAS 1713+53†	17	13	14.2	+53	13	52	20	MID	33	32.4	8.44	16.31	15.07	10.83	11.88
									55	54.1	14.00	14.77			
								NE	5	4.9	5.57	8.19	8.92	10.65[e]	(11.77)
								SW	5	4.9	2.14	2.76	2.69	10.39[e]	(11.24)
MCG–03-57-017	22	28	42.7	–19	17	31	50		5	2.3	10.14	15.61	16.68	10.62[e]	11.25
									17	8.0	22.19	34.78	29.53		
NGC 7469 (UGC 12332)	23	0	44.6	+ 8	36	18	50		5	1.6	52.25	81.18	109.20	10.99	11.59
									17	5.4	75.53	121.97	131.29		
									33	10.6	105.22	167.75	173.07		
									55	17.6	131.25	191.18			
ZW 453.062	23	2	28.1	+19	16	55	40		5	2.4	5.84	8.66	8.75	10.71	11.28
									17	8.1	13.62	16.32	13.62		
									33	15.7	32.37	43.41	37.17		
									55	26.2	38.20	50.88	44.69		
ZW 475.056	23	13	31.2	+25	16	48	30		5	2.7	12.19	17.60	19.69	10.79	11.53
									17	9.0	23.48	32.38	31.31		
									33	17.5	29.89	41.98	37.52		
									55	29.2	32.97	47.20	40.76		
NGC 7592† (Mrk 928)	23	15	47.5	– 4	41	20	35	MID	55	26.0	39.27	52.08	43.47	10.81	11.32
								E	5	2.4	6.34	9.07	8.59	10.46[e]	(11.03)
								W	5	2.4	6.11	8.42	8.06	10.45[e]	(11.00)
NGC 7674† (UGC 12608)	23	25	24.7	+ 8	30	14	45		5	2.8	9.96	16.50	24.79	11.16[e]	11.48
									17	9.5	24.11	34.52	41.14		
									33	18.5	43.46	61.17	66.41		
									55	30.8	57.32	84.40	73.49		
NGC 7771†	23	48	52.1	+19	49	55	110		5	1.4	17.79	27.63	28.20	10.99[e]	11.34
									17	4.8	65.78	95.92	82.84		
									33	9.3	126.50	182.24	152.14		
									55	15.5	190.84	271.48	219.90		
Mrk 331	23	48	52.8	+20	18	22	40		5	1.7	25.95	36.43	34.85	10.63	11.40
									17	5.9	47.22	61.79	54.73		
									33	11.5	61.11	79.41	72.15		
									55	19.2	60.57	82.96	68.27		

[a] The symbol † indicates that a comment regarding that source appears at the end of the table.

[b] Refer to the notes to Table I for an explanation of specific beam positions.

[c] The 5″ and 10″ measurements are from Carico *et al.* (1988).

[d] Parentheses indicate estimates for individual nuclei within sources containing multiple nuclei (see Section III-*b*).

[e] This value of L_* is *not* a reasonable estimate of the total stellar luminosity – the largest available beam diameter was too small.

Notes to TABLE I

(Angular separations given here are only approximate)

MCG − 02-01-051 and MCG + 02-04-025. It was recently discovered that, due to a misidentification in the observing logs, the data reported by Carico *et al.* (1988) for MCG + 02-04-025 were actually measurements of MCG − 02-01-051. Hence, the 5″ measurements reported here for MCG − 02-01-051N, are those previously reported as MCG + 02-04-025(a), and those for MCG − 02-01-051S, are the average of the previously reported measurements for MCG − 02-01-051 and MCG + 02-04-025(b). The designations N and S for MCG − 02-01-051 refer to the two distinct nuclei in a N–S orientation separated by 50″. There are no 5″ measurements available for MCG + 02-04-025.

NGC 1068. The near-infrared data were previously published by Scoville *et al.* (1988).

UGC 2369. There are two visually obvious nuclei in a N–S orientation separated by 30″. The 5″, 17″, and 33″ measurements are of the respective nuclei; the 55″ measurements are of a position midway between the nuclei, encompassing both.

IRAS 0335 + 15. There are two visually obvious nuclei separated by 15″ in an E–W orientation. All measurements are of the E nucleus. Due to the close association of the two nuclei, all measurements with beam diameters greater than 17″ contain emission from the companion (W) nucleus. No attempt has been made to correct for this effect, as this nucleus is considerably fainter than the E nucleus.

MCG − 03-12-002. There are two visually obvious nuclei in a N–S orientation separated by 15″. Thus, although all measurements are centered on the respective nuclei, the 33″ and 55″ measurements of the N nucleus include emission from both nuclei.

IRAS 1056 + 24. There are two nuclei in a NW–SE orientation separated by 10″. All measurements are of the NW nucleus, which is the dominant source.

UGC 6436. There are two visually distinct nuclei in an E–W orientation separated by 20″. The measurements are of the respective nuclei; however, the 55″ measurements contain emission from both nuclei. Hence, the luminosities have been estimated from the 33″ measurements.

NGC 3690. The visual image of this source shows two apparently merging galaxies in an E–W orientation separated by 25″; the galaxy to the W is NGC 3690. The other galaxy, not measured in this analysis, is IC 694.

NGC 4922. There are two visually obvious nuclei in a NE–SW orientation separated by 20″. The 5″, 17″, and 33″ diameter beam measurements are of the respective nuclei; the 55″ diameter beam measurements are centered at a position midway between the two nuclei.

UGC 8335. There are two visually obvious nuclei in a NW–SE orientation separated by 30″. The measurements are of the respective nuclei.

NGC 5256. There are two visually obvious nuclei in a NE–SW orientation separated by 10″. The 5″ measurements are of the SW nucleus; the larger beam measurements are centered midway between the two nuclei, encompassing both.

NGC 5257. This source was reported by Carico *et al.* (1988) as NGC 5257/8; it has since been determined that NGC 5257 along is the *IRAS* source, rather than in combination with NGC 5258, which lies 80″ to the NW.

UGC 9618. There are two merging galaxies in a N–S orientation separated by 40″. There appears to be a bright foreground star roughly midway between the two nuclei, and it is likely that this star is causing the anomalous increase in the 33″ measurements of the N nucleus. For this reason, the luminosities for that nucleus have been estimated from the 17″ measurements.

IRAS 1525 + 36. This object consists of a compact central source, with a diameter of 10″ (~10 kpc), and a faint surrounding ringlike structure extending out to a radius of roughly 20″ (~20 kpc; see Sanders *et al.* 1988). The measurements are consistent with this morphology. However, the 33″ and 55″ beams may also have been contaminated by emission from the nearby galaxy and/or foreground star lying 20″ N and NE, respectively.

NGC 6090. There are two visually obvious nuclei in a NE–SW orientation separated by 10″. The 10″ measurements are of the respective nuclei; the larger beam measurements are centered midway between the two nuclei, encompassing both.

NGC 6286. This source was reported by Carico *et al.* (1988) as NGC 6285/6; it has since been determined that NGC 6286 alone is the *IRAS* source, rather than in combination with NGC 6285, which lies 80″ to the NW.

IRAS 1713 + 53. There are two visually obvious nuclei in a NE–SW orientation separated by 10″. The 5″ measurements are of the respective nuclei; the larger beam measurements are centered midway between the two nuclei, encompassing both.

NGC 7592. There are two visually obvious nuclei in an E–W orientation separated by 10″. The 5″ measurements are of the respective nuclei; the 55″ measurements are centered midway between the two nuclei, encompassing both.

NGC 7674. There are two visually obvious nuclei in a NW–SW orientation separated by 30″. All measurements are of the dominant SW nucleus.

NGC 7771. There are two visually obvious nuclei in a NE–SW orientation separated by 50″. All measurements are of the dominant NE nucleus.

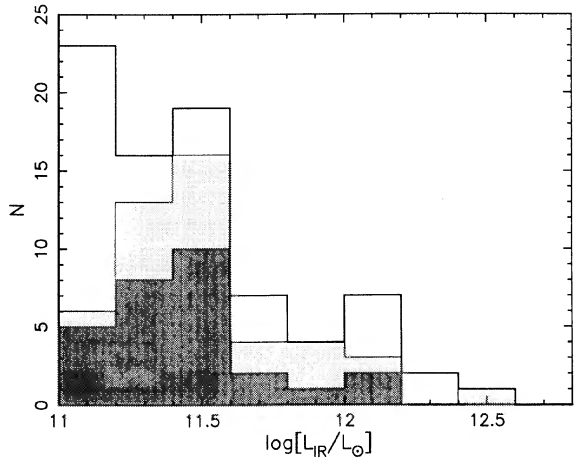

FIG. 1. Distribution of infrared luminosities L_{IR} for three samples of galaxies. The unshaded histogram includes all galaxies from the BG Sample with $L_{IR} \geqslant 10^{11}\ L_{\odot}$. The light-shaded histogram includes only those galaxies from the BG Sample that were observed with multiple beam diameters; these galaxies are listed in Table I. The dark-shaded histogram includes only those galaxies from Table I for which near-infrared colors for *both* the nucleus and the disk were obtainable (see Sec. III*a3*); these galaxies are listed in Table II.

TABLE II. Flux density ratios.

NAME	POS[a]	D_1[b] (kpc)	D_2[b] (kpc)	LOG[$f_\nu(1.6\mu m)/f_\nu(1.3\mu m)$][c] NUCLEUS	DISK	LOG[$f_\nu(2.2\mu m)/f_\nu(1.6\mu m)$] NUCLEUS	DISK
MCG-03-04-014		3.2	21.4	0.16	0.08	-0.01	-0.06
NGC 695		3.2	20.9	0.14	0.08	-0.02	-0.10
NGC 958		1.9	20.5	0.14	0.16	-0.07	-0.09
NGC 1068		0.4	4.8	* 0.19	0.13	0.41	-0.09
UGC 2238		2.0	22.2	* 0.26	0.16	0.06	-0.08
UGC 2369	N	3.0	20.0	0.14	0.10	-0.06	-0.11
UGC 2982		1.7	18.9	* 0.22	0.15	0.00	-0.08
MCG-0312002	N	3.1	20.2	* 0.11	0.11	0.04	-0.15
NGC 1614		1.5	10.1	0.15	0.13	0.00	-0.03
MCG+08-18-012		2.5	16.6	* 0.15	0.11	-0.00	-0.15
NGC 3110		1.6	10.3	0.15	0.12	-0.04	-0.10
A1101+41		3.3	22.1	* 0.16	0.10	0.02	-0.11
UGC 6436	W	3.3	11.2	0.16	0.04	-0.01	-0.04
NGC 4418		0.7	4.4	0.12	0.08	-0.06	-0.12
IC 860		1.3	8.3	0.12	0.09	-0.06	-0.14
NGC 5257		2.2	14.5	0.14	0.11	-0.04	-0.08
Mrk 273		3.7	24.3	* 0.18	0.19	0.07	-0.09
UGC 8739		1.7	10.9	* 0.29	0.18	0.07	-0.07
UGC 9618	N	3.3	21.6	* 0.26	0.12	0.07	-0.05
I ZW 107		3.9	25.7	0.12	0.09	0.03	-0.10
ARP 220		1.8	6.0	* 0.28	0.14	0.10	-0.14
MCG+0142088		2.3	15.1	0.17	0.09	0.00	-0.03
NGC 6286		3.6	12.0	* 0.20	0.16	0.03	-0.11
ZW 453.062		2.4	15.7	* 0.17	0.12	0.00	-0.09
ZW 475.056		2.7	29.2	* 0.16	0.15	0.05	-0.15
NGC 7674		2.8	30.8	* 0.22	0.16	0.18	-0.14
NGC 7771		1.4	15.5	* 0.19	0.15	0.01	-0.10
Mrk 331		1.7	11.5	0.15	0.09	-0.02	-0.06

[a] The beam position in the source; refer to the notes to Table I.

[b] D_1 and D_2 are the inner and outer diameters, respectively, of the annulus used to calculate the colors of the disk; the units are kiloparsecs at the source.

[c] A * preceding the color measurements indicates a source for which the error ellipses for the nuclear and disk colors do *not* overlap; for these sources the nuclear and disk colors are clearly distinct.

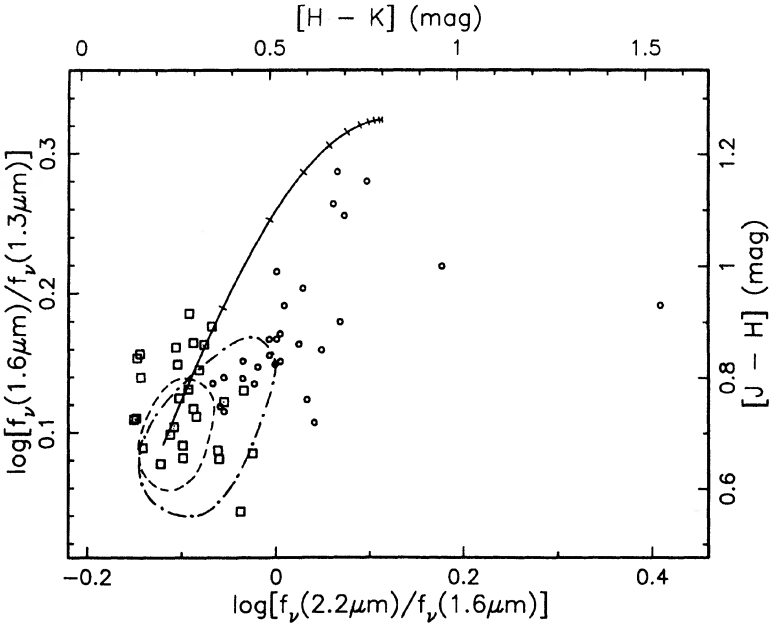

FIG. 2. Near-infrared flux density ratios (colors). The circles are the galaxy nuclei and the squares are the galaxy disks (see text). Only those galaxies which have colors with uncertainties less than 33% for both the nucleus and disk are shown. The dashed line indicates the colors of the normal field spiral galaxies measured by Aaronson (1977), and the dashed–dotted line indicates the colors of a sample of lower luminosity *IRAS* galaxies (Carico *et al.* 1986). The solid line indicates the effect on the colors of a normal galaxy due to extinction from dust mixed with the source; the line extends to a total visual extinction $A_V = 50$ mag, with tick marks at every 5 mag. Typical uncertainties are ± 0.09 for the disks and ± 0.04 for the nuclei.

nearby, generally lower luminosity starburst galaxies. On the other hand, the result shown in Fig. 2 differs significantly from the observed properties of low-luminosity, normal galaxies, which typically show no change in near-infrared colors with beam diameter (Aaronson 1977).

Because of the large uncertainties in the large-beam measurements, those galaxies for which annular colors are obtainable represent the most extended sources in the current sample. Since the most extended sources tend to be those that are closest, and since the BG Sample is a flux-limited sample, it follows that the galaxies plotted in Fig. 2 are biased toward lower luminosities. Figure 1 shows a histogram of the distribution of luminosities for the galaxies included in Fig. 2 compared to similar histograms for all of the galaxies in Table I and all of the galaxies from the BG Sample with $L_{IR} \geqslant 10^{11}\ L_{\odot}$. It is seen that there may be some bias against the highest luminosity galaxies: Fig. 2 includes only two of the ten galaxies from the BG Sample with $L_{IR} \geqslant 10^{12}\ L_{\odot}$, as compared to 26 of the 69 galaxies from the BG Sample with $L_{IR} \geqslant 10^{11}\ L_{\odot}$. However, if the result in Fig. 2 is combined with the results of an analysis of the spatial distribution of the near-infrared emission in nine galaxies from the BG Sample with $L_{IR} \geqslant 10^{12}\ L_{\odot}$ utilizing near-infrared camera images (Carico *et al.* 1990), it is found that four of the ten galaxies with $L_{IR} \geqslant 10^{12}\ L_{\odot}$ have nuclei that are significantly redder than their surrounding disks. This fraction is comparable to the fraction of galaxies with $L_{IR} \geqslant 10^{11}\ L_{\odot}$ in which this effect is seen.

Figure 2 implies that the 2.2 μm emission is more centrally concentrated in infrared luminous galaxies than the 1.3 or 1.6 μm emission. This is investigated further in Fig. 3, where the availability of multiple beam diameter measurements has been utilized by interpolating between beam diameters to obtain estimates of the emission that would have been measured within a specified diameter about each galaxy nucleus. In this way, distance effects have been eliminated by estimating for each source the quantities $f_{\nu}(\lambda)_{d\,\mathrm{kpc}}$, the flux densities that would have been measured with a beam diameter corresponding to a region of diameter d, in kiloparsecs, about the nucleus; the spatial distribution of the near-infrared emission in different sources can then be directly compared.

In Fig. 3, the ratio $f_{\nu}\ (2.2\ \mu\mathrm{m})_{2\,\mathrm{kpc}}/f_{\nu}(2.2\ \mu\mathrm{m})_{10\,\mathrm{kpc}}$ is plotted against the same quantity at 1.3 μm. This ratio is a measure of the compactness of the emission about each nucleus. The line indicates the locus of points for which the ratios at 1.3 and 2.2 μm are equal. Typical uncertainties in the ratios are on the order of 10%–15%, so that many of the points in Fig. 3 are consistent with no wavelength dependence in the compactness of the emission. Nevertheless, the sample taken as a whole clearly indicates a tendency among infrared luminous galaxies toward emission that is more tightly concentrated about the nucleus at 2.2 μm than at 1.3 μm.

In Fig. 4, the analysis of the concentration of the infrared emission has been extended to 10 μm. For this figure, it was not possible to estimate the emission at 10 μm within a region of diameter d in kiloparsecs at the source, since multiple beam diameter measurements are not available for these galaxies at 10 μm. Instead, an estimate of the compactness of the 10 μm emission from Paper I has been used. In that paper, R_{10} was defined as the ratio of the 10 μm emission in a 5″ diameter beam to that which would have been measured at 10 μm in a beam the size of the *IRAS* 12 μm beam; see Paper I for details of how this quantity was determined. At 2.2 μm, a corresponding quantity, $R_{2.2}$, has been calculated for comparison. $R_{2.2}$ is the ratio of the 2.2 μm flux density measured in a 5″ diameter beam divided by the 2.2 μm flux density measured in the largest diameter beam. The straight line is the same as in Fig. 3. The plot shows that, for those galaxies for which the emission is fairly compact, the 10 μm emission is more centrally concentrated than the near-infrared emission.

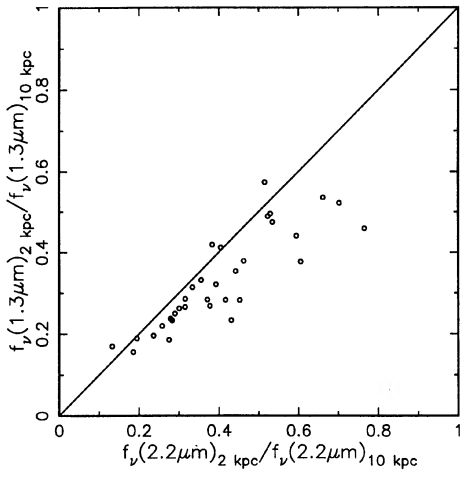

FIG. 3. Concentration of the 1.3 μm emission about the galaxy nucleus, with distance effects removed, plotted against the same quantity at 2.2 μm. $f_{\nu}(\lambda)_{d\,\mathrm{kpc}}$ is an estimate of the flux density that would have been measured with a beam diameter corresponding to a region of diameter d, in kiloparsecs, about the nucleus. The line represents the locus of points for which the concentrations at both wavelengths are equal.

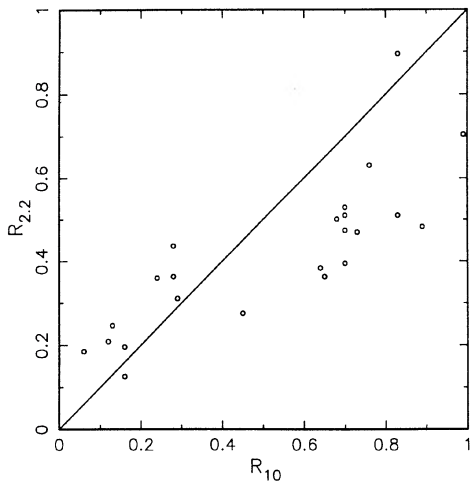

FIG. 4. Concentration of the 10 μm emission about the galaxy nucleus plotted against the concentration of the 2.2 μm emission (see text). The line represents the locus of points for which the concentrations at both wavelengths are equal. The values of R_{10} are from Carico *et al.* (1988).

There is a significant source of uncertainty in the estimates of R_{10} due primarily to the 10 μm silicate absorption feature. No attempt has been made to correct for this effect. Any such correction would tend to increase the values of R_{10}, further strengthening the result seen in Fig. 4. Also, there is some uncertainty in the comparison between R_{10} and $R_{2.2}$ due to the fact that the large diameter beams used in calculating $R_{2.2}$ are considerably smaller than the size of the *IRAS* beam used in calculating R_{10}. However, any correction for this effect would tend to decrease the value of $R_{2.2}$, and thus would also strengthen the result seen in Fig. 4.

The red near-infrared colors of the galaxy nuclei in Fig. 2 cannot be explained in terms of direct or reddened stellar emission, but suggest the presence of hot dust contributing significant emission at wavelengths as short as 2.2 μm (Paper I). Figure 2 suggests, then, that these galaxies have an increased density of dust in their nuclei relative to their outer disks. This conclusion also provides a natural explanation for the result seen in Figs. 3 and 4, since a greater amount of dust in the nucleus would affect the observed spatial distribution of the galaxy emission in the following ways: (1) Extinction by dust of the intrinsic emission would tend to reduce the observed emission from the nucleus more severely than that from the outer disk, thus causing an apparent decrease in the estimated compactness of the emission about the nucleus. Since dust extinction is greater at shorter wavelengths, this would contribute to the result in Figs. 3 and 4. (2) Dust emission from the nucleus would tend to increase the compactness of the emission, and this increase would be more significant at longer wavelengths, where the emission is less contaminated by photospheric emission. This would also contribute to the result in Figs. 3 and 4.

Since the measurements with 5″ and 10″ diameter beams were made by chopping to an angular distance of typically 15″ (Paper I), one would expect that, for many of the sources, the 5″ and 10″ diameter reference beams were contaminated by emission from the extended galaxy. Any such contamination in the smaller diameter beam would tend to reduce the observed compactness of the emission. However, estimates of the amount of flux that would have contaminated the small diameter reference beams for each source indicated that the effect is negligible. Thus, the result seen in Figs. 3 and 4 appears to be a real property of the galaxies.

The conclusion drawn from Figs. 2–4, that the unusually red near-infrared colors seen in many infrared luminous galaxies are confined to the nuclei of those galaxies, and hence that the effects of dust required to explain the red near-infrared colors are also confined to the nuclei, has an important implication for the overall distribution of luminosity within infrared luminous galaxies. Since such galaxies tend to radiate most of their power at far-infrared wavelengths, and since far-infrared emission is generally reradiated emission from dust grains, it is probable that the bulk of the luminosity from infrared luminous galaxies is emitted from their nuclei. Furthermore, since the galaxies in the current sample all have infrared luminosities that exceed the bolometric luminosities of most "normal" galaxies, their nuclei, if the source of the total luminosity, must be characterized by extremely high radiation densities, presumably due to highly intense star-formation activity, or the presence of a central quasar, or both. Confirmation of this idea will require more direct information on the distribution of emission at far-infrared wavelengths than is currently available for these galaxies.

2) 2.2 μm luminosity

The values of $f_\nu(\lambda)_{d\,\mathrm{kpc}}$, from the previous section can be used to estimate $L_\nu(\lambda)_{d\,\mathrm{kpc}}$, the power emitted at wavelength λ from regions of the same size, centered about the nucleus, in each galaxy. The values of $L_\nu(2.2\,\mu\mathrm{m})_{2\,\mathrm{kpc}} \equiv 4\pi D^2 \nu f_\nu(2.2\,\mu\mathrm{m})_{2\,\mathrm{kpc}}$, where D is the luminosity distance, are given in Table III for 39 of the sources. These values were obtained by simply interpolating linearly between the measurements at the relevant beam diameters, or between the smallest available beam diameter and a diameter of zero. Since the curves of growth generally have negative curvatures, these luminosities have been slightly underestimated. Values of $L_\nu(2.2\,\mu\mathrm{m})_{2\,\mathrm{kpc}}$ were calculated for all sources for which the smallest beam diameter is less than 2 kpc. For the remaining sources, $L_\nu(2.2\,\mu\mathrm{m})_{2\,\mathrm{kpc}}$ was calculated only if a linear fit between the smallest available beam diameter and a diameter of zero represented a reasonable extrapolation of the growth curve from the larger beam diameters.

In addition to the galaxies listed in Table I, Table III includes values of $L_\nu(2.2\,\mu\mathrm{m})_{2\,\mathrm{kpc}}$ for seven more galaxies from the BG Sample using data from Carico *et al.* (1990). All of these additional galaxies have infrared luminosities $L_{\mathrm{IR}} \geqslant 10^{12}\ L_\odot$; thus, they belong to the subsample of the BG Sample from which the galaxies in Table I were selected, and have been included in Figs. 5–7 without specific identification.

The distribution of $L_\nu(2.2\,\mu\mathrm{m})_{2\,\mathrm{kpc}}$ for the nuclei in Table III is shown in Fig. 5, and the distribution of the distance-independent estimate of the compactness of the 2.2 μm emission, $L_\nu(2.2\,\mu\mathrm{m})_{2\,\mathrm{kpc}}/L_\nu(2.2\,\mu\mathrm{m})_{10\,\mathrm{kpc}}$ [which is equivalent to the quantity $f_\nu(2.2\,\mu\mathrm{m})_{2\,\mathrm{kpc}}/f_\nu(2.2\,\mu\mathrm{m})_{10\,\mathrm{kpc}}$, previously plotted in Fig. 3], is shown in Fig. 6. In both figures, the unshaded histogram includes all nuclei from Table III, whereas the shaded histogram includes only those sources which are classified in Véron-Cetty and Véron (1989) as Seyfert or quasar nuclei,* or which were identified by Sanders *et al.* (1988) as having an AGN.

Included in Figs. 5 and 6 are estimates of $L_\nu(2.2\,\mu\mathrm{m})_{2\,\mathrm{kpc}}$ and $L_\nu(2.2\,\mu\mathrm{m})_{2\,\mathrm{kpc}}/L_\nu(2.2\,\mu\mathrm{m})_{10\,\mathrm{kpc}}$ for the archetypal "starburst" galaxy NGC 253. These estimates were obtained using the data from the near-infrared mapping of this source by Scoville *et al.* (1985). Also indicated in Fig. 5 is the value of $L_\nu(2.2\,\mu\mathrm{m})_{2\,\mathrm{kpc}}$ for the well-studied Seyfert galaxy NGC 1068, calculated from the data for this source given in Table I. NGC 1068 is also indicated in Fig. 6; however, since the largest available beam diameter corresponds to only 4.8 kpc at the distance of NGC 1068, the estimate of $f_\nu(2.2\,\mu\mathrm{m})_{10\,\mathrm{kpc}}$ was obtained by extrapolating to 10 kpc with an exponential curve fitted to the two largest diameter beams.

If NGC 253 and NGC 1068 are taken to be typical of classical starburst and Seyfert galaxies, respectively, then Figs. 5 and 6 indicate that infrared luminous galaxies are characterized by a significantly higher density of stars and/or interstellar material emitting at 2.2 μm within their nuclei than exists in classical starburst nuclei, and that the density of this 2.2 μm emitting material falls off much more rapidly with radial distance. However, the nuclei in infrared

*Véron-Cetty and Véron (1989) is *not* a complete listing of Seyfert galaxies and/or quasars, but was simply utilized in this analysis as a convenient reference.

TABLE III. Luminosities within fixed physical diameters.

NAME[a]	POS[b]	$\frac{L_\nu(2.2\mu m)_{2\ kpc}}{L_\odot}$ [c]	$\frac{L_\nu(2.2\mu m)_{2\ kpc}}{L_\nu(2.2\mu m)_{10\ kpc}}$ [d]	AGN[e]	NAME[a]	POS[b]	$\frac{L_\nu(2.2\mu m)_{2\ kpc}}{L_\odot}$ [c]	$\frac{L_\nu(2.2\mu m)_{2\ kpc}}{L_\nu(2.2\mu m)_{10\ kpc}}$ [d]	AGN[e]
NGC 34		9.99	0.70	VV/2	Mrk 231		11.23	0.77	VV/Q
MCG-02-01-051	S	9.47	0.44		NGC 4922	SW	9.73	0.36	
	N	8.72	0.13		IC 860		9.17		
MCG-03-04-014		9.89	0.33		UGC 8335	NW	9.43	0.41	
NGC 695		9.79	0.29			SE	9.73	0.52	
NGC 958		9.60	0.19		NGC 5256	SW	9.65		
NGC 1068		10.27		VV/1		NE	9.52		
UGC 2238		9.67	0.45		NGC 5257		9.27	0.19	
UGC 2369	N	9.67	0.30		UGC 8739		9.41	0.27	
	S	9.54	0.38		ZW 247.020		9.64	0.53	
UGC 2982		9.53	0.28		IRAS 14348-1447†	SW	9.66		S88
MCG-03-12-002	N	9.60	0.32			NE	9.45		S88
NGC 1614		9.94	0.52		IRAS 15250+3609†		9.50	0.37	S88
IRAS 05189-2524†		10.66		S88	Arp 220		9.72	0.43	VV/2
NGC 2623		9.63	0.61		MCG+01-42-088		9.72	0.39	
IRAS 08572+3915†		9.70	0.51	S88	NGC 6286		9.59	0.28	
UGC 5101†		10.22	0.92	S88	MCG-03-57-017		9.75		
MGC+08-18-012		9.65	0.59		NGC 7469		10.31	0.66	VV/1
NGC 3110		9.48	0.26		ZW 453.062		9.48	0.38	
A1101+41		9.60	0.37		ZW 475.056		9.87	0.46	
UGC 6436	W	9.57	0.32		NGC 7674		10.00	0.42	VV/2
NGC 3690		9.57			NGC 7771		9.73	0.24	
IRAS 12112+0305†		9.43		S88	Mrk 331		9.90	0.53	
NGC 4418		8.90							

[a] A † indicates sources for which the data from Carico *et al.* (1990) were used in calculated $L_\nu(2.2\mu m)_{2\ kpc}$ and $L_\nu(2.2\mu m)_{2\ kpc}/L_\nu(2.2\mu m)_{10\ kpc}$.

[b] The beam position in the source; refer to the notes to Table I.

[c] The 2.2 μm luminosity emitted from a region about the nucleus 2 kpc in diameter (see text).

[d] The ratio of the luminosities emitted from regions about the nucleus 2 kpc in diameter and 10 kpc in diameter (see text).

[e] Sources listed in Véron-Cetty and Véron (1989) as Seyfert 1 (VV/1), Seyfert 2 (VV/2), or a quasar (VV/Q), or identified by Sanders *et al.* (1988) as having an AGN (S88).

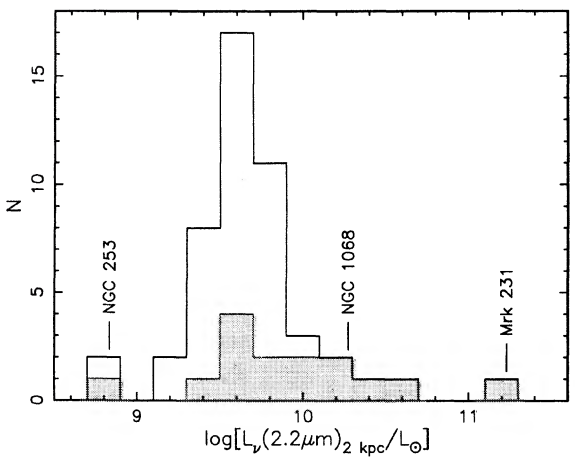

FIG. 5. 2.2 μm luminosity emitted within a region of diameter 2 kpc about each galaxy nucleus. The unshaded histogram is the distribution for all galaxies listed in Table III; the shaded histogram is the distribution for only those galaxies listed in Véron-Cetty and Véron (1989) as Seyferts or quasars, or identified by Sanders *et al.* (1988) as having an AGN. The value of $L_\nu(2.2\ \mu m)_{2\ kpc}$ for the archetypal Seyfert galaxy NGC 1068, included in the current sample, is indicated (see text). Also shown is an estimate of $L_\nu(2.2\ \mu m)_{2\ kpc}$ for NGC 253, obtained from the data of Scoville *et al.* (1985). The medians for the unshaded and shaded histograms are $L_\nu(2.2\mu m)_{2\ kpc} = 4.4\times10^9\ L_\odot$ and $5.2\times10^9\ L_\odot$, respectively.

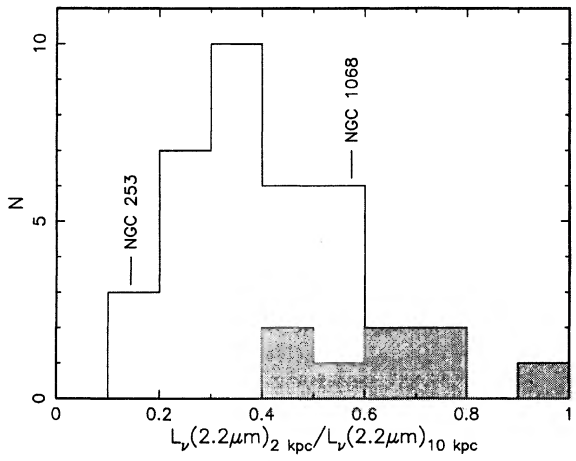

FIG. 6. Concentration of the 2.2 μm emission about the galaxy nucleus, with distance effects removed. $L_\nu\ (2.2\ \mu m)_{2\ kpc}/L_\nu(2.2\ \mu m)_{10\ kpc}$ is defined for each galaxy as the ratio of the 2.2 μm luminosity within a region of diameter 2 kpc about the nucleus to the 2.2 μm luminosity within a region of diameter 10 kpc (see text). The unshaded histogram is the distribution for all galaxies from Table III; the shaded histogram is the distribution for only those galaxies listed in Véron-Cetty and Véron (1989) as Seyferts or quasars, or identified by Sanders *et al.* (1988) as having an AGN. Also shown are estimates of $L_\nu(2.2\ \mu m)_{2\ kpc}/L_\nu(2.2\ \mu m)_{10\ kpc}$ for NGC 253, obtained from the data of Scoville *et al.* (1985), and for NGC 1068 (see text). The medians for the unshaded and shaded histograms are $L_\nu(2.2\ \mu m)_{2\ kpc}/L_\nu(2.2\ \mu m)_{10\ kpc} = 38\%$ and 63%, respectively.

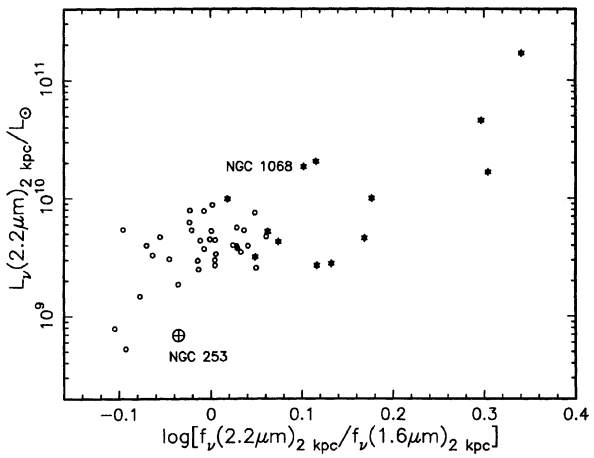

FIG. 7. Logarithm of the 2.2 μm luminosity within a region of diameter 2 kpc about the nucleus, plotted against the logarithm of the ratio f_ν $(2.2\,\mu m)_{2\,kpc}/f_\nu(1.6\,\mu m)_{2\,kpc}$. Galaxies classified in Véron-Cetty and Véron (1989) as Seyfert galaxies, or identified by Sanders *et al.* (1988) as having an AGN, are plotted as the filled hexagons. Included is the starburst galaxy NGC 253, its position on the plot having been estimated from the data of Scoville *et al.* (1985).

luminous galaxies are typically *not* as luminous at 2.2 μm, nor is their 2.2 μm emission as centrally concentrated, as that of classical Seyfert galaxies.

This result suggests that, if the intrinsic source of the high luminosity in these galaxies is star formation, then the star-formation activity in their nuclei must be extremely intense. Alternatively, the luminosities in a number of sources may be due to, or at least enhanced by, the presence of a dust-enshrouded quasar. The existence of a quasar energy source is fairly well established in at least two of the sources: Mrk 231, which is actually listed as a quasar in Véron-Cetty and Véron (1989) (see also the discussion and references in Sec. III*a3* below), and NGC 7469, which is known to have a Seyfert 1 nucleus (Osterbrock 1977) [see, for example, Weedman (1986) for a discussion of the correspondence between Seyfert 1 nuclei and quasars]. The fact that several other galaxies in the sample have 2.2 μm emission comparable in strength and compactness to one or both of these sources suggests that other galaxies in the sample, particularly those listed in Table III as Seyfert 2 or identified by Sanders *et al.* (1988) as having an active nucleus, may also be powered by a quasar. Large amounts of dust in an AGN could cause enough extinction to reduce significantly the observed 2.2 μm nuclear luminosity (see the discussion of Arp 220 and NGC 4418 in Sec. III*a3* below), and may be the reason that a number of known "infrared Seyferts" included in Fig. 5 have such low 2.2 μm luminosities in their nuclei. However, the evidence for quasar nuclei remains ambiguous, and other emission mechanisms cannot be ruled out, even for the highest luminosity sources (see, e.g., Riecke 1988; Harwit *et al.* 1987).

The relation between the distribution of the 2.2 μm luminosity and the spatial variation of the near-infrared colors is investigated in Fig. 7, where $L_\nu(2.2\,\mu m)_{2\,kpc}$ is plotted against the logarithm of the ratio $f_\nu(2.2\,\mu m)_{2\,kpc}/f_\nu(1.6\,\mu m)_{2\,kpc}$, which is the color calculated from the 2.2 and 1.65 μm flux densities within a diameter of 2 kpc about the center of each nucleus. The correlation apparent in this figure indicates that the physical mechanism responsible for the red near-infrared colors seen in the nuclei of many of the infrared luminous galaxies is coupled with an increase in 2.2 μm emitting material in those nuclei relative to other, less red nuclei. This is obviously consistent with, though not identical to, the results of Sec. III*a1*, which postulated an increased density of hot dust emitting at 2.2 μm to account for the color gradient between the galaxy nuclei and their outer disks. Whereas Fig. 2 shows that unusually red near-infrared colors in a galaxy imply a higher concentration of hot dust in that galaxy's nucleus relative to its own outer disk, Fig. 7 indicates that those colors also imply a higher concentration of hot dust in that galaxy's nucleus relative to other galaxy nuclei.

3) Individual sources

The source that stands out most strikingly in Figs. 5 and 6 and Table III is Mrk 231. This is not surprising since this source, listed as a quasar in Véron-Cetty and Véron (1989), has long been known as an extremely luminous, compact galaxy (Young, Knacke, and Joyce 1972; Rieke and Low 1972). With a 2.2 μm luminosity, of greater than 10^{11} $L_\odot$ within a radius of 1 kpc from its center, its nucleus is nearly an order-of-magnitude more luminous at 2.2 μm than that of NGC 1068, and is *250 times* more luminous than the nucleus of NGC 253. In fact,the nuclear near-infrared properties of Mrk 231 are considerably more extreme in comparison to other infrared luminous galaxies than are the properties of its integrated longer wavelength emission. For comparison, the total infrared luminosity L_{IR} of Mrk 231 is only a factor of 2 greater than that of Arp 220, the second most luminous galaxy in the current sample, whereas its nuclear 2.2 μm luminosity, L_ν $(2.2\,\mu m)_{2\,kpc}$, is more than a factor of 30 greater than that of Arp 220.

These considerations are easily understood in terms of dust extinction in the nuclei of the infrared Seyferts. For a galaxy with a large amount of dust in its nucleus, such as Arp 220 or NGC 4418 (see the discussion below), much of the near-infrared emission from within the nucleus would be absorbed and reradiated at far-infrared wavelengths, reducing the observed 2.2 μm nuclear luminosity. In contrast, for a galaxy with relatively little dust obscuring the central AGN in comparison to other infrared Seyferts, as Sanders *et al.* (1988) have suggested is the case for Mrk 231, the energy distribution would more closely resemble the flat distribution typical of a classical quasar, in which a greater fraction of the total luminosity is seen at near-infrared wavelengths than is typical of infrared luminous galaxies.

In addition to Mrk 231, a number of other sources stand out in Figs. 5 and 6. Those nuclei forming the high-luminosity "tail" in Fig. 5, and hence emitting exceedingly high 2.2 μm luminosities from their nuclei, are Mrk 231, IRAS 05189 − 2524, NGC 7469, NGC 1068, UGC 5101, NGC 7674, NGC 34, and NGC 1614. Mrk 231, NGC 7469, NGC 1068, and NGC 7674 are all well-studied Seyfert galaxies listed in Véron-Cetty and Véron (1989), and IRAS 05189 − 2524 and UGC 5101 have been studied extensively by Sanders *et al.* (1988), who identified them both as having Seyfert nuclei as well. Hence, the extremely high nuclear luminosities for these galaxies are not surprising. NGC 34 is also classified in Véron-Cetty and Véron as a Seyfert galaxy, but seems to have received very little attention to date. An

(unpublished) image of this source at 6500 Å, taken by the authors, shows a single bright nucleus, with a single tail-like structure extending ~ 15 kpc away from it, which may suggest that this source is a completed merger (compare optical images of IRAS 05189 − 2524 and Mrk 231 from Sanders *et al.*). This source may be an extremely interesting candidate for further observation.

NGC 1614, although not a Seyfert, was recognized many years ago as an unusual galaxy, with very high luminosity, strong emission lines, and a compact core (Ulrich 1972, and references therein; Rieke and Low 1972). Aitken, Roche, and Phillips (1981) suggested that the infrared emitting region in this source has a diameter $\lesssim 1.5$ kpc, and from an analysis presented in Paper I it was found that as much as 80% of the 10 μm emission from this galaxy could be coming from a point source in the nucleus. From these considerations, it is also not surprising that this source has a value of $L_\nu(2.2\,\mu\text{m})_{2\,\text{kpc}}$ that is among the highest in the current sample.

The sources forming the tail at the high end of the distribution in Fig. 6, and hence having unusually compact 2.2 μm emission, are UGC 5101, Mrk 231, NGC 34, NGC 7469, and NGC 2623. The first four have already been discussed and have Seyfert nuclei, which accounts for their highly compact emission. However, NGC 2623, which has been studied extensively (see, e.g., Joy and Harvey 1987; Baan *et al.* 1985; Casoli *et al.* 1988), has an optical spectrum that shows no indication of a Seyfert nucleus, and it is not clear from previously published work why this source is so compact at 2.2 μm. It is possible, however, that it contains an AGN that is too heavily shrouded in dust to be identifiable at visible wavelengths; a similar situation is believed to exist in a number of infrared luminous galaxies, including Arp 220 (Norris 1985; Graham *et al.* 1990) and NGC 4418 (see Roche *et al.* 1986, and the discussion below). Indeed, such a possibility seems reasonable given the conclusions of Joy and Harvey that NGC 2623 is the remnant of a completed merger with $\sim 90\%$ of its luminosity emitted by dust.

Finally, NGC 4418, listed in Véron-Cetty and Véron (1989) as a *possible* Seyfert galaxy, holds a distinct position in the current sample in that, despite this possible Seyfert classification, it has the second *least* luminous nucleus at 2.2 μm, and is significantly extended at 2.2 μm out to a diameter of at least 4 kpc (the largest 2.2 μm beam diameter for this source; see Table I). NGC 4418 was studied by Roche *et al.* (1986), who found that it has a compact 10 μm source ($\lesssim 0.5$ kpc in diameter) containing a tremendous amount of absorbing material, responsible for a visual extinction $A_V \gg 50$ mag which renders the nucleus virtually invisible at optical wavelengths. This unusually high extinction can be predicted simply on the basis of the ratio of infrared to visible luminosities (a measure of the total luminosity reradiated by dust compared to the observable, hence unabsorbed, intrinsic luminosity), which, for this galaxy, is ~ 50, placing it at the very highest end of this ratio, not only for the current sample of galaxies, but for the entire BG Sample (see Soifer *et al.* 1989). It is probable that the low 2.2 μm luminosity in this galaxy's nucleus is due to dust extinction at 2.2 μm, which shifts the bulk of the observed emission to far-infrared wavelengths. All of these considerations are reminiscent of Arp 220, which also has a compact infrared core of diameter $\lesssim 0.5$ kpc (Becklin and Wynn-Williams 1987; Graham *et al.* 1990) containing a (double) active nucleus (Norris 1985; Graham *et al.* 1990) heavily enshrouded by dust, responsible for a visual extinction ~ 50 mag (Becklin and Wynn-Williams), an extremely high (~ 150) infrared-to-visible luminosity ratio (Soifer *et al.* 1987), and an extended 2.2 μm luminosity profile (Table I). This suggests that NGC 4418 may be a less luminous version of Arp 220, in which case it would also be an interesting object for further study.

b) Total Near-Infrared Emission

The large diameter beam measurements provide an opportunity to estimate the total near-infrared emission in a large sample of high-luminosity *IRAS* galaxies. The optical diameter of the galaxies in the current sample, using visual estimates from the Palomar Observatory Sky Survey prints (Paper I), has a median of 35″ and a maximum of 540″. Thus, although a 55″ diameter beam may not include the total emission in some sources, it should provide a good estimate for the majority. This is also indicated by the curves of growth, from which it is clear that, for the majority of the galaxies, the total flux outside the 33″ diameter beam is a small fraction of the total flux (the median 1.65 μm flux density in a 33″–55″ annulus is $\sim 20\%$ of that inside the 33″ diameter beam).

The luminosity at 1.65 μm (the H wavelength band) can be used as an estimate of the total near-infrared luminosity, where $L_H \equiv 4\pi D^2 \nu f_\nu(1.65\ \mu\text{m})$, D is the luminosity distance, and $f_\nu(1.65\,\mu\text{m})$ is the flux density measured with the largest available beam diameter. The blue luminosity, $L_B \equiv 4\pi D^2 \nu f_\nu(0.43\,\mu\text{m})$, can be obtained for each galaxy from the data of Soifer *et al.* (1987). It is then found that the ratio L_H/L_B has a median of 1.9 for the galaxies in Table I, and ranges from a minimum of 0.7 (for NGC 34) to a maximum of 8.5 (for UGC 2982). For this analysis, those galaxies have been excluded for which the largest available beam diameter is too small, as determined from the 1.65 μm curve of growth, to provide a reasonable estimate of the total near-infrared emission; these galaxies are indicated in Table I, in the listing of L_* (see below). A histogram of the values of L_H/L_B for the current sample is shown in Fig. 8.

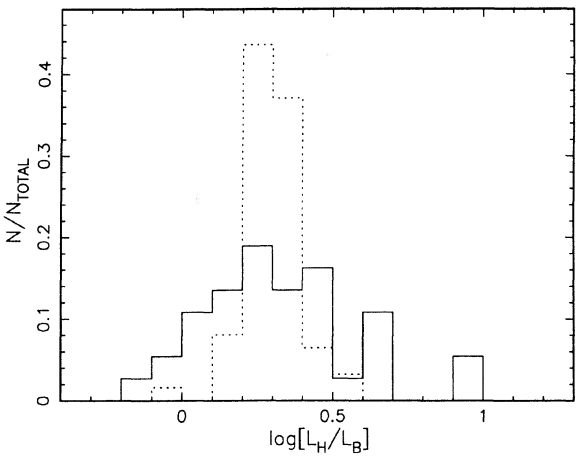

FIG. 8. Ratio of total near-infrared to visible luminosity, L_H/L_B (see text). The solid-line histogram is the distribution for the galaxies listed in Table I; the dotted-line histogram is the distribution for a sample of low-luminosity, optically selected spiral galaxies measured by Aaronson (1977).

These values of L_H/L_B can be compared to those for lower luminosity galaxies by using the sample of 71 optically selected spiral galaxies measured by Aaronson (1977). Estimates of L_H/L_B for the Aaronson sample, the distribution of which is also shown in Fig. 8, were obtained using the magnitudes at H (1.65 μm) and V (0.55 μm) given by Aaronson, and interpolating the V magnitudes to the B wavelength band (0.43 μm) using $B - V = 0.8$ mag, as given by de Vaucouleurs (1959) for spiral galaxies. The distribution has a median of 2.0, and ranges from a minimum of 1.0 to a maximum of 3.8. The measurements presented by Aaronson were typically done with beam diameters representing a considerably smaller fraction of the galaxy diameter than the measurements presented here. However, Aaronson has shown that the galaxies in his sample exhibit no significant change in galaxy colors with beam diameter.

As seen in Fig. 8, the range of values of L_H/L_B for the galaxies measured by Aaronson (1977) is considerably narrower than the range of values for the galaxies listed in Table I, indicating the more uniform emission properties expected for a sample of normal galaxies. However, the fact that the median values of L_H/L_B for the two samples are virtually identical demonstrates that the global near-infrared luminosity does not trace the infrared activity in galaxies, a result which provides further evidence that the processes responsible for the unusual properties of infrared luminous galaxies are confined to the nuclear regions.

The estimates of the total near-infrared emission can also be used to estimate the contribution of the stellar luminosity to the total energy budget of infrared luminous galaxies. The stellar luminosity L_* is taken to be $4\pi D^2(F_B + F_{\rm NIR})$, where D is the luminosity distance, $F_B \equiv \nu f_\nu(0.43\,\mu{\rm m})$, and $F_{\rm NIR}$ is an estimate of the stellar near-infrared emission obtained by fitting a single-temperature blackbody curve to the near-infrared colors for a typical, normal spiral galaxy (Aaronson 1977) and integrating the flux under this curve, normalized to the 1.65 μm flux density from the largest available beam size, for each galaxy. The values of L_* are listed in Table I, along with the values of $L_{\rm IR}$ from Paper I. Galaxies for which L_* is *not* a reasonable estimate of the total stellar emission, based on a 1.65 μm growth curve which is still increasing significantly at the largest available beam diameter, have been flagged with a footnote, and were excluded from the analysis. For sources with obvious double nuclei, estimates of $L_{\rm IR}$ for each nucleus were obtained by assuming that each nucleus contributes the same fraction of the total luminosity at far-infrared wavelengths as at 2.2 μm, where the fraction contributed at 2.2 μm was calculated from the largest available beam size, unless otherwise noted. These estimates for individual nuclei are shown in parentheses in Table I.

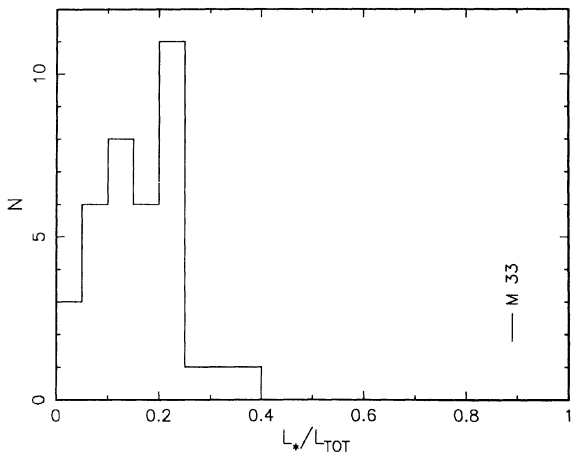

FIG. 9. Distribution of the fraction of the total luminosity attributable to stellar emission in infrared luminous galaxies, defined as the ratio of the stellar luminosity L_*, as estimated from the blue luminosity and the 1.65 μm flux density (see text), to the total luminosity $L_{\rm TOT} \equiv L_* + L_{\rm IR}$. An estimate for the low-luminosity spiral galaxy M33, calculated from the data in Rice *et al.* (1990), is also shown.

A histogram of the logarithm of $L_*/L_{\rm TOT}$ is shown in Fig. 9, where $L_{\rm TOT} \equiv L_* + L_{\rm IR}$. The figure indicates that the observed stellar luminosity in infrared luminous galaxies is typically $\lesssim 25\%$ of the total luminosity; for the galaxies in Fig. 9, the fraction ranges from a minimum of $\sim 3\%$ (for Arp 220) to a maximum of $\sim 37\%$ (for UGC 6436, east nucleus). For comparison, data from Rice *et al.* (1990) give $L_*/L_{\rm TOT} = 0.89$ for the nearby low-luminosity spiral galaxy M33.

IV. SUMMARY

Forty-seven galaxies from the *IRAS* Bright Galaxy Sample with infrared luminosities $L_{\rm IR} \geqslant 10^{11}\ L_\odot$ have been observed at near-infrared wavelengths with multiple large-diameter beams.

a) Observational Results

(1) The unusually red near-infrared colors known previously for many of these galaxies are confined to their nuclei, within regions typically 1–3 kpc in diameter, whereas the outer disk regions have colors which are essentially those of a normal stellar population.

(2) The 2.2 μm luminosity emitted from the nuclei of infrared luminous galaxies is generally considerably higher and more compact than that seen in classical "starburst" nuclei, but lower and more extended than that seen in classical Seyfert nuclei.

(3) The ratio of near-infrared to visible emission for infrared luminous galaxies, calculated from the *total* near-infrared and visible luminosities for each galaxy, is, on average, comparable to that for low-luminosity, optically selected galaxies.

(4) The observed stellar emission contributes generally $\lesssim 25\%$ of the observed bolometric luminosity in infrared luminous galaxies. This is considerably less than in typical low-luminosity galaxies ($\sim 90\%$ in M33).

b) Interpretation

The effects of dust, reddening, and thermal reradiation, required to explain the observed unusual near-infrared colors, are confined primarily to the nuclei. Since the far-infrared emission is reradiated emission from dust grains, it is probable that the far-infrared luminosity, and hence the bulk of the entire luminosity of infrared luminous galaxies, tends to be strongly concentrated about their nuclei. Thus, *the physical processes responsible for the unusual properties of infrared luminous galaxies tend to be confined to the nuclear regions, with diameters $\lesssim$ 1–3 kpc.* This, together with the

observation that the 2.2 μm nuclear luminosities of these galaxies are generally higher than those of typical starburst nuclei, implies that the nuclei of infrared luminous galaxies must be characterized by exceedingly high radiation densities that are presumably due to extremely intense star formation activity, and in at least some cases, the presence of a central dust-enshrouded quasar. It is suggested that dust extinction at 2.2 μm is the cause of the comparatively low 2.2 μm nuclear luminosities in a number of galaxies contained in the current sample and identified in the literature as having Seyfert nuclei, and that other galaxies in the sample may also have active nuclei buried in their dusty cores.

Since most of the near-infrared luminosity is concentrated in the nuclei of infrared luminous galaxies, it follows that their global near-infrared properties are poor tracers of their infrared activity, which is why the ratio of total near-infrared to visible emission is similar to that for normal, low-luminosity galaxies. Furthermore, since the luminosity source in infrared luminous galaxies is enshrouded in dust, it is not surprising that the observed stellar emission from infrared luminous galaxies is only a minor fraction of the total observed luminosity.

Two galaxies from the current sample appear to be extremely interesting sources for further observation. One of these, NGC 34, has received very little attention in the literature, although it has a Seyfert nucleus and is among the galaxies with the highest 2.2 μm nuclear luminosities and the most compact near-infrared emission. The other galaxy, NGC 4418, appears distinct in the current analysis in that it has one of the *least* luminous nuclei at 2.2 μm despite its identification in the literature as having many of the characteristics of a Seyfert galaxy. It is suggested that this source may be a low-luminosity version of Arp 220.

Special thanks are given to S. E. Persson for the use of his infrared photometer, and to Dave Tennent, John Henning, and Mike Doyle for their much needed help in getting it all working. Thanks are also given to the night assistants at the Palomar 60 in. telescope, Russ Day, Will McKinley, Jeff Phinney, and Skip Staples, and the entire staff at Palomar Observatory. A number of useful comments and references were provided by the anonymous referee, and we greatly appreciate his/her time and effort in reviewing this work. The Palomar 60 in. telescope is owned jointly by the California Institute of Technology and the Carnegie Institution of Washington. Ground-based astronomy at Caltech is supported by a grant from the National Science Foundation.

REFERENCES

Aaronson, M. (1977). Ph.D. thesis, Harvard University.
Aitken, D. K., Roche, P. F., and Phillips, M. M. (1981). Mon. Not. R. Astron. Soc. **196**, 9p.
Baan, W. A., Haschick, A. D., Buckley, D., and Schmelz, J. T. (1985). Astrophys. J. **293**, 394.
Becklin, E. E., and Wynn-Williams, C. G. (1987). In *Star Formation in Galaxies*, edited by C. J. Lonsdale (U.S. GPO, Washington, DC), p. 643.
Boulanger, F., Beichman, C., Désert, F. X., Helou, G., Pérault, M., and Ryter, C. (1988). Astrophys. J. **332**, 328.
Carico, D. P., Graham, J. R., Matthews, K., Wilson, T. D., Soifer, B. T., Neugebauer, G., and Sanders, D. B. (1990). Astrophys. J. Lett. **349**, L39.
Carico, D. P., Sanders, D. B., Soifer, B. T., Elias, J. H., Matthews, K., and Neugebauer, G. (1988). Astron. J. **95**, 356 (Paper I).
Carico, D. P., Soifer, B. T., Beichman, C., Elias, J. H., Matthews, K., and Neugebauer, G. (1986). Astron. J. **92**, 1254.
Casoli, F., Combes, F., Dupraz, C., Gerin, M., Encrenaz, P., and Salez, M. (1988). Astron. Astrophys. **192**, L17.
Cutri, R. M., Rudy, R. J., Rieke, G. H., Tokunaga, A. T., and Willner, S. P. (1984). Astrophys. J. **280**, 521.
de Vaucouleurs, G. (1959). Handb. Phys. **53**, 275.
Devereux, N. A. (1989). Astrophys. J. **346**, 126.
Graham, J. R., Carico, D. P., Matthews, K., Neugebauer, G., Soifer, B. T., and Wilson, T. D. (1990). Astrophys. J. Lett. (in press).
Harwit, M., Houck, J. R., Soifer, B. T., and Palumbo, G. G. C. (1987). Astrophys. J. **315**, 28.
Helou, G. (1986). Astrophys. J. Lett. **311**, L33.
Infrared Astronomical Satellite (*IRAS*) *Catalogs and Atlases*: *Explanatory Supplement* (1988). Edited by C. A. Beichman, G. Neugebauer, H. J. Habing, P. E. Clegg, and T. J. Chester (NASA, Washington, DC).
Joy, M., and Harvey, P. M. (1987). Astrophys. J. **315**, 480.
Norris, R. P. (1985). Mon. Not. R. Astron. Soc. **216**, 701.
Osterbrock, D. E. (1977). Astrophys. J. **215**, 733.
Phinney, E. S. (1989). In *Theory of Accretion Disks*, edited by W. Duschl, F. Meyer, and J. Frank (Kluwer, Dordrecht), p. 457.
Rice, W., Boulanger, F., Viallefond, F., Soifer, B. T., and Freedman, W. L. (1990). Astron. J. (in press).
Rieke, G. H. (1988). Astrophys. J. Lett. **331**, L5.
Rieke, G. H., and Low, F. J. (1972). Astrophys. J. Lett. **176**, L95.
Roche, P. F., Aitken, D. K., Smith, C. H., and James, S. D. (1986). Mon. Not. R. Astron. Soc. **218**, 19p.
Sanders, D. B., Phinney, E. S., Neugebauer, G., Soifer, B. T., and Matthews, K. (1989). Astrophys. J. **347**, 29.
Sanders, D. B., Scoville, N. Z., Young, J. S., Soifer, B. T., Schloerb, F. P., Rice, W. L., and Danielson, G. E. (1986). Astrophys. J. Lett. **305**, L45.
Sanders, D. B., Soifer, B. T., Elias, J. H., Madore, B. F., Matthews, K., Neugebauer, G., and Scoville, N. Z. (1988). Astrophys. J. **325**, 74.
Scoville, N. Z., Matthews, K., Carico, D. P., and Sanders, D. B. (1988). Astrophys. J. Lett. **327**, L61.
Scoville, N. Z., Soifer, B. T., Neugebauer, G., Young, J. S., Matthews, K., and Yerka, J. (1985). Astrophys. J. **289**, 129.
Soifer, B. T., Boehmer, L., Neugebauer, G., and Sanders, D. B. (1989). Astron. J. **98**, 766.
Soifer, B. T., Sanders, D. B., Madore, B., Neugebauer, G., Danielson, G. E., Elias, J. H., Persson, C. J., and Rice, W. L. (1987). Astrophys. J. **320**, 238.
Telesco, C. M., Decher, R., and Joy, M. (1989). Astrophys. J. Lett. **343**, L13.
Ulrich, M. (1972). Astrophys. J. **178**, 113.
Véron-Cetty, M. P., and Véron, P. (1989). *A Catalog of Quasars and Active Nuclei*, 4th ed. (European Southern Observatory, München).
Weedman, D. W. (1986). *Quasar Astronomy* (Cambridge University, Cambridge).
Young, E. T., Knacke, R. F., and Joyce, R. R. (1972). Nature **238**, 263.